International Journal of
Applied Ceramic TECHNOLOGY

ORIGINAL ARTICLE

Photoluminescent and antimicrobial properties of silver-doped indium hydroxide synthesized by one-step microwave-assisted hydrothermal method

Nivaldo Freire Andrade Neto[1] (iD) | Mara T. S. Tavares[2] | Erik A. C. Ferreira[1] | Ana I. L. Sales[3] | Lucymara F. A. Lima[3] | Elson Longo[4] | Mauricio R. D. Bomio[1] | Fabiana V. Motta[1]

[1]LSQM, DEMAT, UFRN, Natal, Brazil

[2]IFBA, Feira de Santana, Feira de Santana, Brazil

[3]LBMG, UFRN, Natal, Brazil

[4]LIEC, UFSCar, São Carlos, Araraquara, Brazil

Correspondence
Nivaldo Freire Andrade Neto, LSQM, DEMAT, UFRN, Natal, Brazil.
Email: nfandraden@gmail.com

Funding information
FAPESP-CDMF, Grant/Award Number: 2013/07296-2; CNPq; CAPES

Abstract

Silver-doped indium hydroxide $In_{(1-x)}(OH)_3$:$_x$Ag (with $x = 0$, 1, 2, 4, and 8 mol %) of Ag nanoparticles were synthesized by the microwave-assisted hydrothermal (MAH) method at 140°C for 30 minutes. These nanoparticles were characterized by X-ray diffraction (XRD), fourier transformed infrared (FT-IR) spectroscopy, and optical diffuse reflectance. Photoluminescence (PL) spectra were acquired with a 350 nm beam of a krypton ion laser as an excitation source. The antibacterial activities of the samples were evaluated against gram negative *Escherichia coli* bacteria and gram positive *Staphylococcus aureus* bacteria using the disc diffusion method. The results showed that all diffraction peaks present in XRD patterns could be indexed to the cubic lattice related to the $In(OH)_3$ phase. Broadband photoluminescence behavior in visible range spectra was observed for all samples with a maximum peak centered in the blue and green regions. The antibacterial activities showed that $In_{(1-x)}(OH)_3$: $_x$Ag nanoparticles have a promising bactericide that can be used for deactivating microbes.

KEYWORDS

bactericide activity, doping, indium hydroxide, microwave, silver

1 | INTRODUCTION

In recent years, several papers report that different types of food and environmental sources harbor bacteria that are resistant to one or more antibiotics.[1,2] Therefore, any search of new methods that minimize or delete food contamination will have a significant impact on the incidence of food-borne diseases.[3] A possible approach is using nanoparticle materials to reduce the microbial contamination on the food surfaces and in the food preparation environment. Nanomaterials are efficient, since they are able to attach more copies of microbial assemblage and cells.[4] Nanostructures presented unique properties, which are different from bulk materials, having enhanced properties and technological applications.[5–7]

Silver nanoparticles have shown their efficacy as an alternative antimicrobial material over a wide diversity of bacteria. Dai et al[8] showed that nanoparticles of AgCl/Ag have a good antibacterial effect against *Escherichia coli* (ATCC 25922), *Staphylococcus aureus* (ATCC 29213), *Staphylococcus epidermidis* (ATCC 12228), *Pseudomonas aeruginosa* (ATCC 15692), and one fungal species *Candida albicans* (CAF2/1). Due to these properties, they can be added to medical materials aimed at preventing infections.[9] Ag particles at a nanometer scale have a higher chemical activity due to their greater area

ratio by its volume, and have drawn an increasing attention to it,[10,11] resulting in the appearance of new mechanical, chemical, electrical, optical, magnetic, electro-optical, and magneto-optical properties of the nanoparticles, which are different from their bulk properties.[12] Studies reported the antibacterial activity of Ag nanoparticles with different modifications.[11,13] The antimicrobial activity increases as the size of the Ag nanoparticles decreases.[14] However, silver nanoparticles with diameters <200 nm have high surface energy, consequently they tend to aggregate spontaneously to reduce this energy, making them unstable for long-term applications in air, water or sunlight.[15] To solve this problem, a wide range of materials, such as ZnO,[16,17] TiO$_2$,[18,19] and SiO$_2$[20,21] have been employed as a support for Ag nanoparticles, so that the ultra fine Ag nanoparticles can be homogeneously formed without aggregation.[22] Among the numerous semiconductors, the use of In(OH)$_3$ is not reported in literature. This semiconductor has a wide (Eg) gap estimated to be 5.15 eV,[23,24] especially at nanostructure sizes, and has created intensive interest because of its semiconducting and optical properties.

In summary, this study reports the synthesis of In$_{(1-x)}$(OH)$_3$:$_x$Ag structures doped with $x = 0, 1, 2, 4,$ and 8 mol% of Ag using the MAH method at the low temperature of 140°C for 30 minutes. In addition, the antimicrobial activity and photoluminescent properties of Ag-doped In(OH)$_3$ particles were investigated to enlarge our understanding of their fundamental properties (Table 1).

2 | EXPERIMENTAL

2.1 | Materials

Indium nitrate (In(NO$_3$)$_3$·H$_2$O, 99%; Sigma-Aldrich, St. Louis, MO), silver nitrate (AgNO$_3$, 99%; Fluka Mumbai, India), potassium hydroxide (KOH, Fluka, 99%), and distilled water were used as received to prepare silver-doped indium hydroxide nanoparticles.

2.2 | Preparation of In(OH)$_3$ nanoparticles

The experimental procedure is as follows: 7 mmol of indium nitrate and silver nitrate were dissolved into 80 mL of deionized water under constant stirring for 20 minutes. Ag was added to it in the following percentages: 0, 1, 2, 4, and 8 mol%. The pH of the solution was adjusted to 11 by adding potassium hydroxide (6 mol/L). The mixture was transferred into a teflon autoclave which was sealed, and the reaction system was heated under hydrothermal conditions at 140°C for 30 minutes (the heating rate was fixed at 25C°/min) using microwave irradiation (2.45 GHz and a maximum power of 800 W). The pressure in the autoclave

TABLE 1 Lattice constants (a, Å), cell volumes (V, Å^3) and the average crystallite size (D_{crys}, Å) of the cubic structure of In(OH)$_3$:$_x$Ag powders prepared by the microwave-assisted hydrothermal method

In(OH)$_3$:$_x$Ag	a (Å)	V (Å^3)	D (nm)
$x = 0$	7.97	505.9	3.20
$x = 1\%$	7.95	503.7	2.94
$x = 2\%$	7.94	503.1	1.93
$x = 4\%$	7.93	501.5	1.85
$x = 8\%$	7.92	499.8	1.81

was stabilized at 3.0 atm. The white product obtained by the microwave-assisted hydrothermal (MAH) treatment was centrifuged, washed with distilled water and ethanol and finally dried at room temperature.

2.3 | Characterization of In(OH)$_3$ nanoparticles

The powders were characterized by X-ray diffraction (XRD) using a Shimadzu diffractometer (Model XRD-7000, CuKα radiation [$\lambda = 1.54$ Å], 40 kV and 30 mA and 2θ from 5° to 80°; Shimadzu, Tokyo, Japan). FT-IR spectra were taken in the range from 4000 to 450 cm^{-1} using KBr pellets as a reference using a Perkin–Elmer FT-IR 1000 spectrophotometer in its transmittance mode. The In(OH)$_3$ morphology and particle size were observed by FEG-SEM (Supra 35-VP Model; Carl Zeiss, Jena, Germany). UV–vis reflectance spectra of In(OH)$_3$ pure and doped powders were taken using Shimadzu (model UV-2600) spectrophotometer. All measurements were taken at room temperature.

2.4 | Photoluminescence

Photoluminescence (PL) spectra were acquired with an Ash Monospec 27 monochromator (Thermal Jarrel, Franklin, MA) and a R4446 photomultiplier (Hamamatsu Photonics, Hamamatsu, Japan). The 350 nm beam of a krypton ion laser (90 K; Coherent Innova, Santa Clara, CA) was used as an excitation source while maintaining its maximum output power at 200 mW. All measurements were performed at room temperature.

2.5 | Antimicrobial tests

The in vitro antibacterial activity of Ag-doped In(OH)$_3$ nanoparticles were tested against the bacterial species *S. aureus* and *E. coli* by the agar disc diffusion method.[25] Initially, the stock cultures of bacteria were revived by inoculating in broth media and grown at 37°C for 18 hours. The agar plates of media (10 g peptone-, 10 g

NaCl and 5 g yeast extract, 20 g agar in 1000 mL of distilled water) were prepared and wells were made on the plate. Each plate was inoculated with 18-hour-old cultures (100 μL) and spread evenly on the plate. After the samples $In_{(1-x)}(OH)_3$:xAg ($x = 0$, 0.01, 0.02, 0.04, 0.08) were placed onto well plates in triplicate. All the plates were incubated at 37°C for 24 hours and the diameters of the inhibition zone were noted.

3 | RESULTS AND DISCUSSION

X-ray diffraction patterns of $In(OH)_3$ particles with different percentages of Ag prepared by the MAH method at 140°C for 30 minutes are shown in Figure 1A-E, respectively. All diffraction peaks in XRD patterns could be indexed to the cubic lattice related to the $In(OH)_3$ phase (PDF card N°. 16-161). With the increase in percentages of silver (see Figure 1B–D), all phases obtained by the MAH treatment remained as $In(OH)_3$ with a cubic structure which indicates that Ag ions were incorporated into $In(OH)_3$ nanocrystals. The presence of secondary phases of AgO and Ag° was not observed, which indicates that the final particles are a pure phase compound.

The crystalline sizes were estimated by the Scherrer equation and full-width half maximum (FWHM) of an observed peak, respectively. The strongest peak (200) was used to calculate the average crystallite size (D) of $In(OH)_3$ particles. The intensity of the peaks was decreased (Figure 1) and the position of the peaks slightly changed to the right (higher angles) with the increase in the silver

concentration, which indicates that Ag^+ doping can cause a slight decrease in the lattice parameters with the $In(OH)_3$[26] doping. The addition of silver promotes the reduction of the parameter a for the $In(OH)_3$ powders, where this reduction is evident when comparing the samples of pure $In(OH)_3$ and doped with 8% Ag, which have parameters a = 7.97 and 7.92Å, respectively. The decrease in the lattice parameters of doped samples is a strong indication that the ions are incorporated into the sites of $In(OH)_3$. These results are in agreement with the investigation realized by Sena et al[27] using the density functional theory (DFT). Sena et al[27] showed in their work that the lattice parameters obtained from the fit for samples of In_2O_3 doped with Fe, Co, and Ni at room temperature are smaller than the lattice parameters for the pure In_2O_3 samples.

The crystallite size decreased with Ag doping level, from 3.20 nm for pure $In(OH)_3$ to 1.81 nm for 8 mol% Ag. These changes are associated with increased disorder in the crystal structure of $In(OH)_3$ by defects caused due to the incorporation of ions with larger ionic radius ($In^{3+} = 0.81$ Å; $Ag^+ = 1.15$ Å) suggesting that the peaks have a greater width according to the Scherrer equation. By increasing the dopant content of Ag^+, the growth of the crystal size was inhibited, this reduction in the crystal size may also be attributed to the formation of In–O–Ag products on the surface of the $In(OH)_3$:Ag, which inhibits the crystal growth.[28]

XPS was used to analyze the as prepared $In(OH)_3$:xAg samples, which is shown in Fig. 2. Symmetrical O 1s peak with binding energy of 531.5 eV can be early in Fig. 2a.[29] The In $3d_{5/2}$ peak with the binding energy of 444 eV (Fig. 2b) confirm that the surface of the material is composed of $In(OH)_3$.[30] The Ag $3d_{5/2, 3/2}$ peaks with binding energy of 367.5 and 374 eV can be early in Fig 2c.[31] The appearance of Ag 3d peaks confirms the substitution of cations In^{3+} by Ag^+.

Additional structural characterization was performed by infrared spectroscopy on the $In_{(1-x)}(OH)_3$:xAg samples. Figure 3A-E shows the FTIR spectra in the transmission mode ranging from 4000 to 450 cm^{-1}. The broad band in the range 3500–2750 cm^{-1} is due to the OH stretching vibrations.[32] The absorption bands observed at 855 cm^{-1} and 776 cm^{-1} for $In(OH)_3$ are attributed to the plane deformation and vibrations in the δIn–OH liberation mode. The absorption bands due to the bridging and terminal hydroxyl groups of indium hydroxide appeared at 1152 and 1060 cm^{-1}, respectively.[33] Other absorption bands between 1377 and 503 cm^{-1} are assigned to In–OH groups.[34] It is observed that the intensity of the respective peaks belongs to the $In(OH)_3$ decrease toward disappearance by increasing the percentage of Ag. Such features are in agreement with XRD data and also indicate that MAH is effective in the synthesis of single phase of Ag-doped $In(OH)_3$ powders.
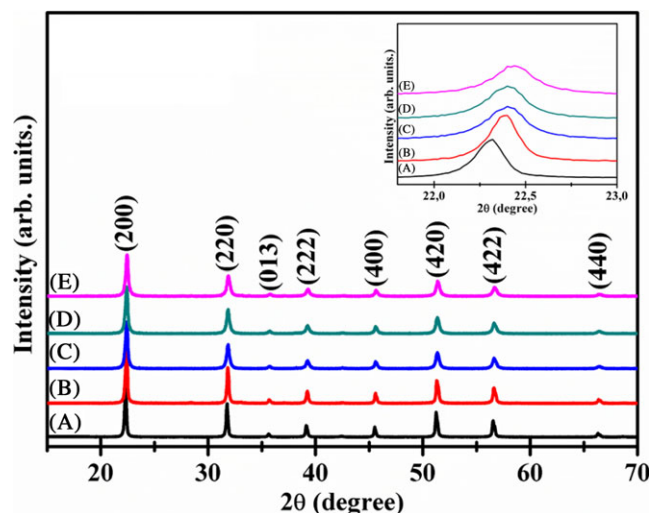

FIGURE 1 X-ray diffraction patterns of $In(OH)_3$:xAg powders obtained by microwave-assisted hydrothermal method at 140°C for 30 min: (A) $x = 0$, (B) $x = 1\%$, (C) $x = 2\%$, (D) $x = 4\%$ and (E) $x = 8\%$ mol. The peaks (200) are shown in inset [Color figure can be viewed at wileyonlinelibrary.com]
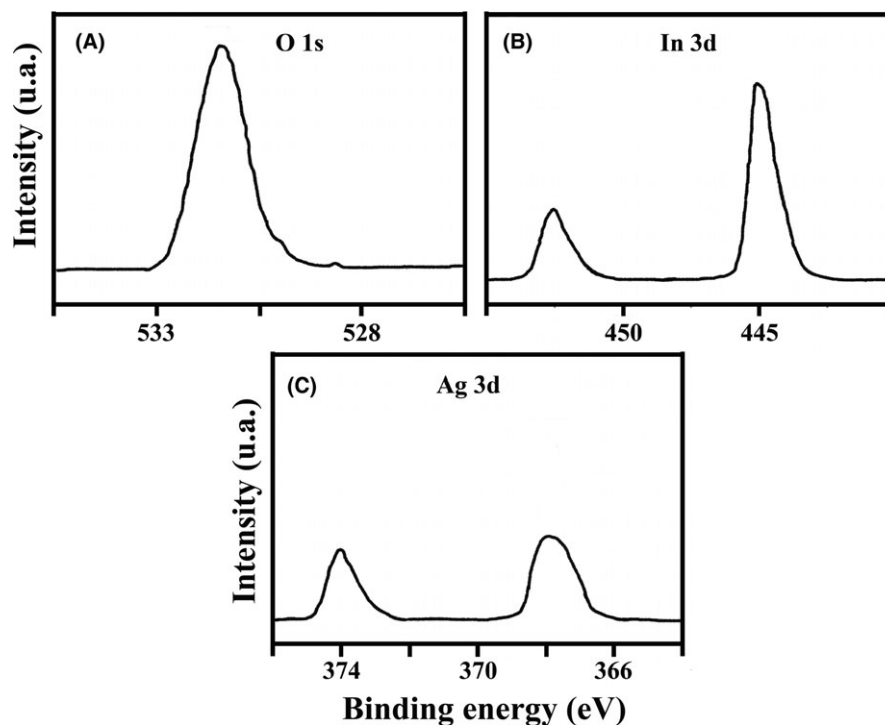
FIGURE 2 XPS spectra of In(OH)$_3$:4%Ag; (A) O 1s peak; (B) In 3d peak; (C) Ag 3d peak

The particle size and morphology of the as-synthesized samples were characterized by FEG-SEM (Figure 4A-E). Figure 4A displays the pure In(OH)$_3$ image where a morphology of microcubes with irregularly shaped structures is visible, which shows that a large amount of microcubes was successfully obtained using the MAH treatment, according to the literature.[35–39] In this study, the cube-shaped morphology was obtained in a short reaction time (30 minutes) which demonstrates the high capability of MAH in obtaining the In(OH)$_3$.

The images showed that with the increased concentration of Ag$^+$ ion, the samples are composed of aggregated particles with medium-sized decrease and irregular morphology (Figure 4B-E). These changes in morphology can be attributed to the principle the nucleation-dissolution-recrystallization mechanism, where the cubic structures of In(OH)$_3$ are dissolved and recrystallized in a different morphology due to the presence of Ag^{3+} inside of its structure.[40] The energy-dispersive X-ray spectra mapping was done in the sample In$_{(0.96)}$(OH)3:$_{(0.04)}$Ag, Figure 3F, in order to prove the chemical composition and the presence of Ag$^+$ ions in the sample.

UV–Vis measurements of In$_{(1-x)}$(OH)$_3$:$_x$Ag samples were also examined by optical diffuse reflectance. The optical band gap estimation was obtained using the Wood and Tauc equation.[41] The estimated optical band values as a function of Ag$^+$ concentration were 5.30, 5.24, 5.20, 5.17, and 5.15 eV for the samples treated at 140°C for

30 minutes for pure In(OH)$_3$ and with 1%, 2%, 4%, and 8% Ag, respectively. A comparison of the pure In(OH)$_3$ (5.30 eV) and In(OH)$_3$: 8% Ag (5.15 eV) illustrates that the increase in the percentage of ion Ag$^+$ ions causes a reduction in the E_{gap} (Figure 5). The reduction in the gap energy is related to the alteration of the network parameters, causing oxygen vacancies, which allow the formation of intermediate levels in the transition band.[42]

The PL emission spectra of the samples were examined at an excitation wavelength of 350 nm (Figure 6). The pure In(OH)$_3$ sample showed maximum peak at 458 nm. Yan et al[43] showed a wide photoluminescent emission in the region of blue and green at 480 nm, in In(OH)$_3$ nanocubes synthesized by the conventional hydrothermal method. The Ag$^+$-doped samples were decomposed into five bands: blue, green, yellow, orange, and red. For the sample with 1% Ag the predominant band is also the blue color with peak maximum in 458 nm. In the samples with 2%, 4%, and 8% Ag the increase in the intensity of the bands occurs in the region of the colors yellow, orange, and red. However, the bands reached a maximum emission at 537, 595, and 575 nm, respectively, which is attributed to the presence of Ag$^+$ in the samples.[43]

Silver clusters are collective oscillations of their electrons in the conduction band, which are known as resonance localized surface plasmon (RPSL). Therefore, electronic property of noble metals, which manifests itself in the visible region of the spectrum electromagnetic, can
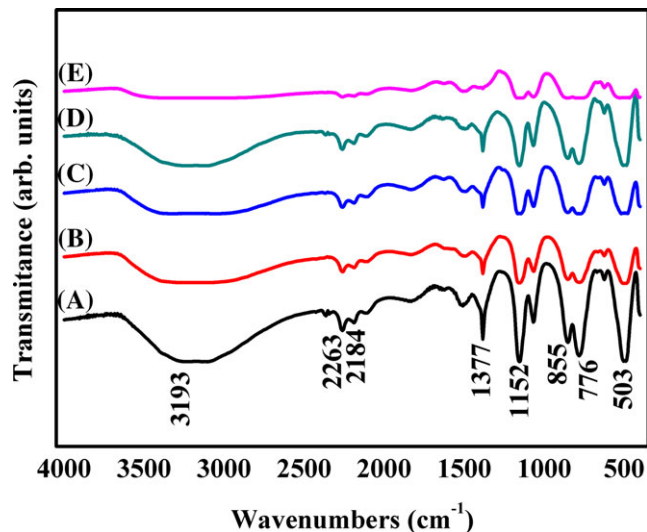
ANDRADE NETO ET AL.

International Journal of
Applied
Ceramic
TECHNOLOGY

475

FIGURE 3 FTIR spectra of $In(OH)_3$:$_x$Ag powders obtained by microwave-assisted hydrothermal method at 140°C for 30 min: (A) $x = 0$, (B) $x = 1\%$, (C) $x = 2\%$, (D) $x = 4\%$ and (E) $x = 8\%$ mol [Color figure can be viewed at wileyonlinelibrary.com]

also be regarded as an optical property. The defects in the particle $[In(OH)_3]_d$ form an association with the clusters $[Ag_4]^x$, or association between $In(OH)_3$ and Ag. The plasmodium model is associated to the semiconductor, where the most important event occurs on the surface of RPSLs, and refers to the electron transfer process between the metal and the semiconductor. In this case, electrons are transferred to the semiconductor, leaving holes in the metal which can contribute to the photocatalytic activity and play an important role in determining the reactivity and stability of the clusters.

The activation mechanism of complex clusters $[Ag_4]^x$ and activation $[In(OH)_3]_d$ with oxygen depend primarily on complex clusters with the formation of peroxide and/or hydroxyl radical. Thus, the holes (h·) generated by "clusters" of Ag $[Ag_4]^x$ can provide favorable conditions for recombination events, electron (e')/hole (h·). Silver has the ability to transfer holes and electrons, producing oxygen radicals and peroxides, by breaking the water molecules, producing a hydroxide radical.
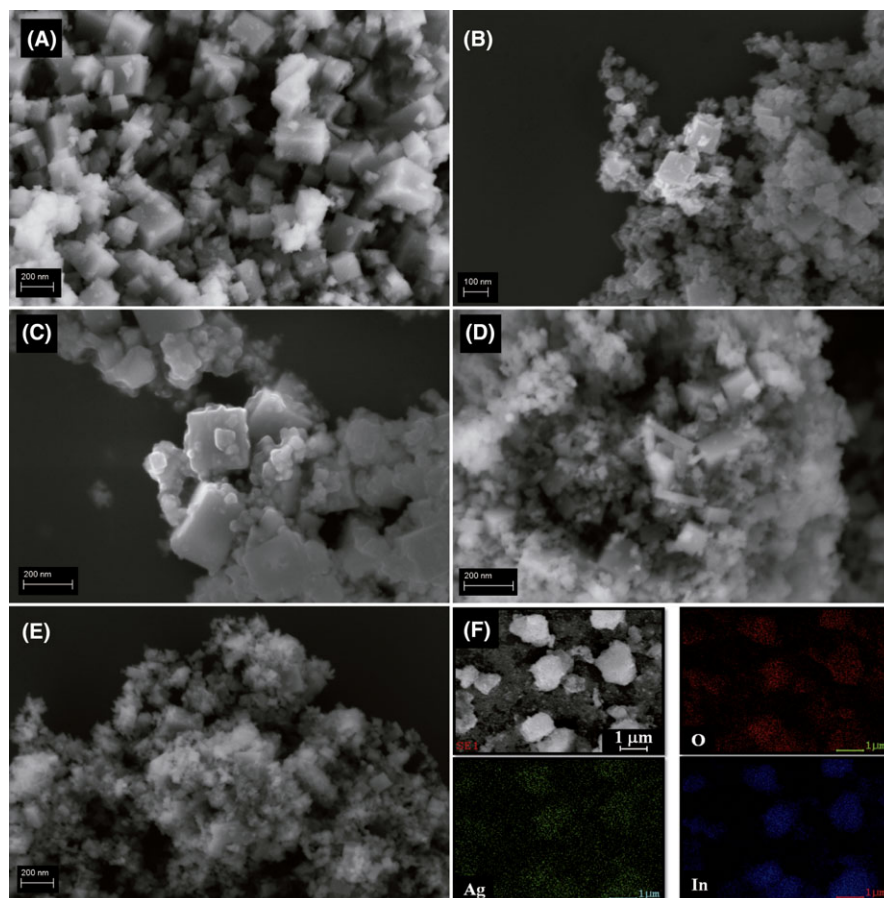

FIGURE 4 FE-SEM images of $In(OH)_3$:$_x$Ag powders: (A) $x = 0$, (B) $x = 1\%$, (C) $x = 2\%$, (D) $x = 4\%$ and (E) $x = 8\%$ mol and (F) mapping the sample $x = 4\%$ [Color figure can be viewed at wileyonlinelibrary.com]
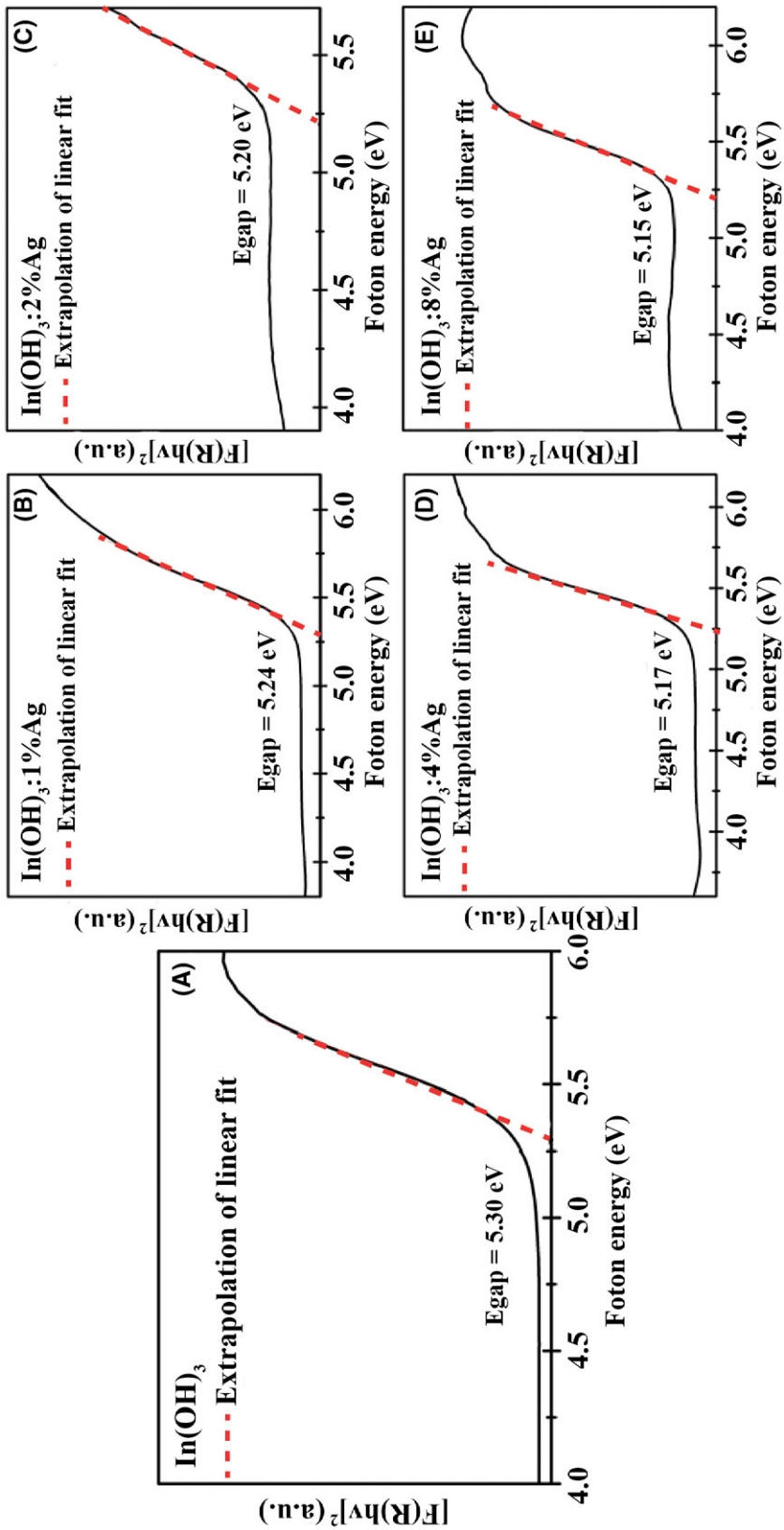
FIGURE 5 UV–Vis absorbance spectra for the In(OH)$_{3-x}$Ag powders obtained by microwave-assisted hydrothermal method at 140°C for 30 min: (A) $x = 0$, (B) $x = 1\%$, (C) $x = 2\%$, (D) $x = 4\%$ and (E) $x = 8\%$ mol
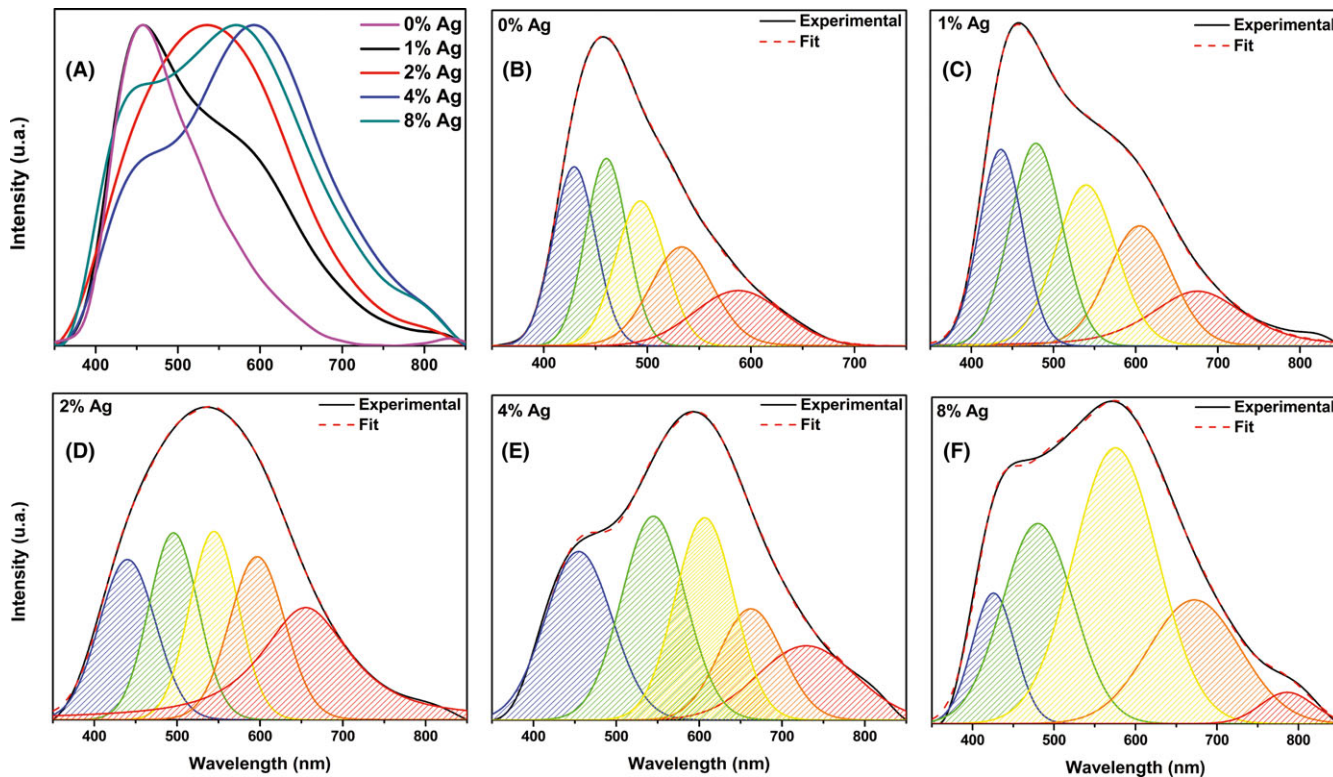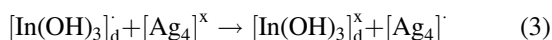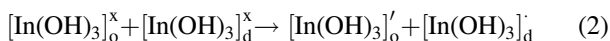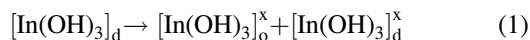
FIGURE 6 (A) Photoluminescence (PL) and deconvolution of the PL emission curves of the In(OH)$_3$:$_x$Ag powders (B) $x = 0$, (C) $x = 1\%$, (D) $x = 2\%$, (E) $x = 4\%$ and (F) $x = 8\%$ mol [Color figure can be viewed at wileyonlinelibrary.com]
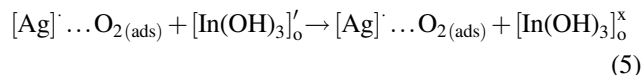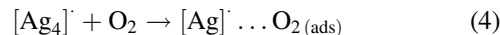
TABLE 2 Mean diameter and standard deviation of the inhibition halos obtained for In(OH)$_3$:$_x$Ag

In(OH)$_3$:$_x$Ag	*Escherichia coli*	*Staphylococcus aureus*
$x = 0$	No inhibition	No inhibition
$x = 1\%$	16 mm (± 0.17)	12.3 mm (± 0.15)
$x = 2\%$	12 mm (± 0.15)	11 mm (± 0.12)
$x = 4\%$	14 mm (± 0.10)	13.3 mm (± 0.19)
$x = 8\%$	14 mm (± 0.12)	13.3 mm (± 0.10)

Both $\left[\text{In(OH)}_3\right]_o^x$ (clusters ordered)/$\left[\text{In(OH)}_3\right]_d^x$ (clusters *disorderly*)as the $\left[\text{AgO}_4\right]^x$ can create hydroxyl radicals (OH·) and the superoxide radical (O$_2^-$) by electron/hole reactions that facilitate inactivation of proteins and any cells. Additionally, an effective charge separation requires an electric field between the sample mass and the cell surface. Therefore, the effect of the surface properties on the performance of reaction electrons/hole should be considered in terms of the following:

$$[\text{In(OH)}_3]_d \rightarrow [\text{In(OH)}_3]_o^x + [\text{In(OH)}_3]_d^x \quad (1)$$

$$[\text{In(OH)}_3]_o^x + [\text{In(OH)}_3]_d^x \rightarrow [\text{In(OH)}_3]_o' + [\text{In(OH)}_3]_d^{\cdot} \quad (2)$$

$$[\text{In(OH)}_3]_d^{\cdot} + [\text{Ag}_4]^x \rightarrow [\text{In(OH)}_3]_d^x + [\text{Ag}_4]^{\cdot} \quad (3)$$

where $\left[\text{In(OH)}_3\right]_d^{\cdot}$ are distorted clusters located in the intermediate energy levels near the valence band (BV) and $\left[\text{In(OH)}_3\right]_o'$ are ordered clusters located in the intermediate energy levels below the conduction band. The reactivity of the oxygen molecule with the complex clusters [Ag$_4$]· results in a kind of silver chemically active surface and, consequently, the incorporation of oxygen in the network:

$$[\text{Ag}_4]^{\cdot} + \text{O}_2 \rightarrow [\text{Ag}]^{\cdot} \ldots \text{O}_{2\,(\text{ads})} \quad (4)$$

$$[\text{Ag}]^{\cdot} \ldots \text{O}_{2\,(\text{ads})} + [\text{In(OH)}_3]_o' \rightarrow [\text{Ag}]^{\cdot} \ldots \text{O}_{2\,(\text{ads})} + [\text{In(OH)}_3]_o^x \quad (5)$$

The clusters formed by the complex silver also interact with water and split it into hydroxyl radicals and hydrogen ions according to the following reactions:

$$[\text{Ag4}]^{\cdot} + \text{H}_2\text{O} \rightarrow [\text{Ag}_4]^{\cdot} \ldots \text{H}_2\text{O}_{(\text{ads})} \quad (6)$$

$$[\text{Ag}_4]^{\cdot} \ldots \text{H}_2\text{O}_{(\text{ads})} \rightarrow [\text{Ag}_4]^{\cdot} \ldots \text{OH}^{\cdot}_{(\text{ads})} + \text{H} \quad (7)$$
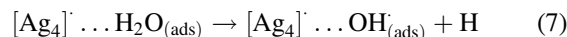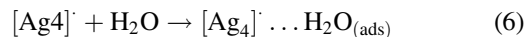
The products of the partial oxidation reaction between water and the complex cluster [Ag$_4$]· are hydroxyl radicals, OH*, and hydrogen ions. These radicals exhibit high oxidation power (which produce a microorganism
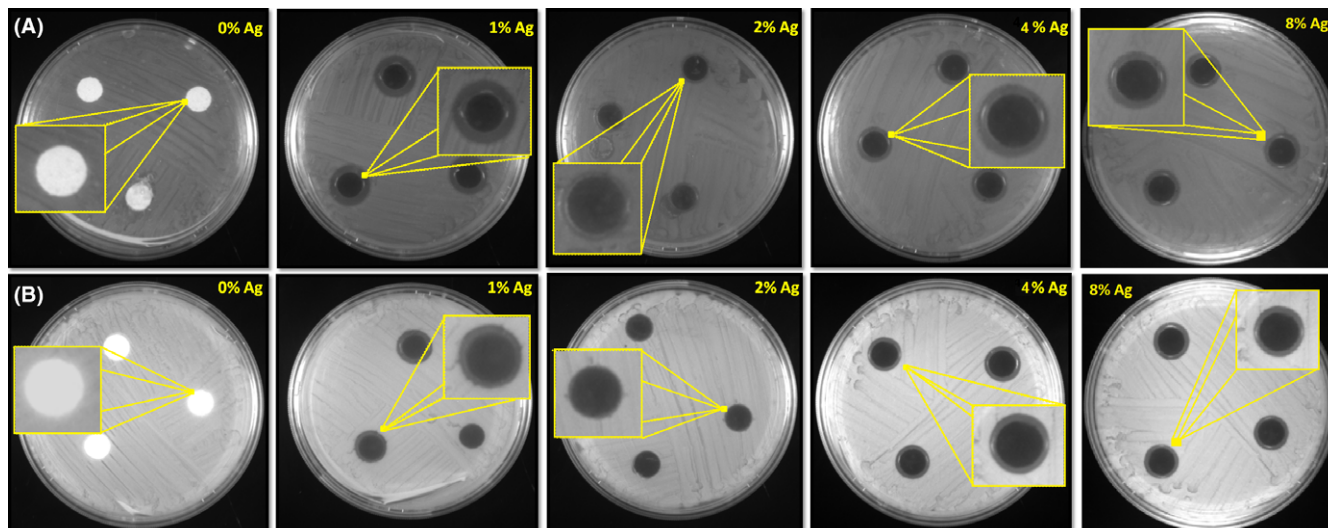
FIGURE 7 Photos of agar plates inoculated with bacteria (A) *Escherichia coli* and (B) *Staphylococcus aureus*, with different concentration of Ag [Color figure can be viewed at wileyonlinelibrary.com]

mineralization in water (anodic oxidation; Equation (5)). The primary cathodic reaction is the formation of superoxide species $[AgO_4]\cdot\ldots O'_2$. Then, these species react with H· and produce hydrogen peroxide radicals ($O_2H\cdot$) via the following reactions:

$$[AgO_4]^{\cdot}\ldots O'_{2\,(ads)} + H^{\cdot} \rightarrow [AgO_4]^{\cdot} + O_2H^{*} \qquad (8)$$
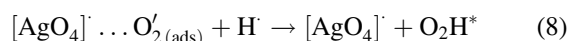
The radicals $OH^{\cdot}$ and $O_2H^{\cdot}$ continue to occur while reacting with the bacterial cells that ultimately result in oxidation.

The antibacterial activity of the prepared samples was tested against gram negative *E. coli* and gram positive *S. aureus* bacteria using the disc diffusion method. Figure 7 shows photographs of the antibacterial tests and the results obtained are summarized in Table 2.

The presence of an inhibition zone clearly indicates the antibacterial effect of the samples doped with Ag for both types of bacteria (*E. coli* and *S. aureus*), while the samples of pure $In(OH)_3$ do not exhibit any antibacterial effect (Figure 7). According to the literature,[44] the low rate of recombination of photogenerated electrons and holes on the surface of the material is the key factor for good bactericide properties. This association with noble metal clusters changes the antibacterial action.

Although the obtained data show that all samples doped with Ag presents a larger antibacterial activity against gram negative (*E. coli*) when compared to gram positive (*S. aureus*) bacteria, this difference is not significant. Therefore, $In(OH)_3$-doped Ag nanoparticles could be useful and effective in bactericidal applications, and it would present a reasonable alternative for the development of new bactericides.

4 | CONCLUSIONS

$In_{(1-x)}(OH)_3{:}_x Ag$ particles (where $x = 0$, 1, 2, 4, and 8 mol %) were efficiently obtained in their crystalline phase using the MAH method at 140°C for 30 minutes. The single phase was obtained at a low temperature and a short synthesis time. The SEM results showed that the cubes are pure indium hydroxide, which is the typical characteristic of the $In(OH)_3$ cubic structure. The use of silver resulted in the collapsing of the cubes. The increase in Ag^+ promotes an increase in the intensity of the broadband in the colors yellow, orange and red which allows it to be considered as a promising material for optical properties. Antibacterial activity tests against *E. coli* and *S. aureus* showed that $In(OH)_3$ particles doped with Ag^+ present antibacterial properties. Although the data obtained show that all samples doped with Ag^+ exhibit a higher antibacterial activity against *E. coli* bacteria (gram negative) when compared with *S. aureus* (gram positive), this difference is not significant. Therefore, the particles $In_{(1-x)}(OH)_3{:}_x Ag$ can be useful and effective in antibacterial applications, and present a reasonable alternative for the development of new antibacterial agents.

ORCID

Nivaldo Freire Andrade Neto http://orcid.org/0000-0003-1421-2904

REFERENCES

1. Anderson AD, Nelson JM, Rossiter S, Angulo FJ. Public health consequences of use of antimicrobial agents in food animals in the United States. Microb Drug Resist. 2003;9(4):373–9.

2. Schroeder CM, White DG, Meng J. Retail meat and poultry as a reservoir of antimicrobial-resistant *Escherichia coli*. Food Microbiol. 2004;21(3):249–55.

3. Byrne CM, Bolton DJ, Sheridan JJ, McDowell DA, Blair IS. The effects of preslaughter washing on the reduction of *Escherichia coli* O157:H7 transfer from cattle hides to carcasses during slaughter. Lett Appl Microbiol. 2000;30(2):142–5.

4. Luo PG, Stutzenberger FJ. Nanotechnology in the detection and control of microorganisms. Adv Appl Microbiol. 2008;63:145–81.

5. Zinatloo-Ajabshir S, Salavati-Niasari M. Novel poly(ethyleneglycol)-assisted synthesis of praseodymium oxide nanostructures via a facile precipitation route. Ceram Int. 2015;41(1, Part A):567–75.

6. Mortazavi-Derazkola S, Zinatloo-Ajabshir S, Salavati-Niasari M. Novel simple solvent-less preparation, characterization and degradation of the cationic dye over holmium oxide ceramic nanostructures. Ceram Int. 2015;41(8):9593–601.

7. Mortazavi-Derazkola S, Zinatloo-Ajabshir S, Salavati-Niasari M. New sodium dodecyl sulfate-assisted preparation of Nd2O3 nanostructures via a simple route. RSC Adv. 2015;5(70):56666–76.

8. Dai L, Liu R, Hu L-Q, Si C-L. Simple and green fabrication of AgCl/Ag-cellulose paper with antibacterial and photocatalytic activity. Carbohydr Polym. 2017;174:450–5.

9. Yao X, Zhang X, Wu H, Tian L, Ma Y, Tang B. Microstructure and antibacterial properties of Cu-doped TiO2 coating on titanium by micro-arc oxidation. Appl Surf Sci. 2014;292:944–7.

10. Wu T-S, Wang K-X, Li G-D, Sun S-Y, Sun J, Chen J-S. Montmorillonite-supported Ag/TiO2 nanoparticles: an efficient visible-light bacteria photodegradation material. ACS Appl Mater Interfaces. 2010;2(2):544–50.

11. Park MVDZ, Neigh AM, Vermeulen JP, de la Fonteyne LJJ, Verharen HW, Briedé JJ, et al. The effect of particle size on the cytotoxicity, inflammation, developmental toxicity and genotoxicity of silver nanoparticles. Biomaterials. 2011;32(36):9810–7.

12. Whitesides GM. Nanoscience, nanotechnology, and chemistry. Small. 2005;1(2):172–9.

13. Devi P, Patil SD, Jeevanandam P, Navani NK, Singla ML. Synthesis, characterization and bactericidal activity of silica/silver core–shell nanoparticles. J Mat Sci Mater Med. 2014;25(5):1267–73.

14. Baker C, Pradhan A, Pakstis L, Pochan DJ, Shah SI. Synthesis and antibacterial properties of silver nanoparticles. J Nanosci Nanotechnol. 2005;5(2):244–9.

15. Cao S, Chen J, Hu J. The fabrication and progress of core-shell composite materials. Aust J Chem. 2009;62(12):1561–76.

16. Zhang Y, Gao X, Zhi L, Liu X, Jiang W, Sun Y, et al. The synergetic antibacterial activity of Ag islands on ZnO (Ag/ZnO) heterostructure nanoparticles and its mode of action. J Inorg Biochem. 2014;130:74–83.

17. Motshekga SC, Ray SS, Onyango MS, Momba MNB. Microwave-assisted synthesis, characterization and antibacterial activity of Ag/ZnO nanoparticles supported bentonite clay. J Hazard Mater. 2013;262:439–46.

18. Bokare A, Sanap A, Pai M, Sabharwal S, Athawale AA. Antibacterial activities of Nd doped and Ag coated TiO2 nanoparticles under solar light irradiation. Colloids Surf B Biointerfaces. 2013;102:273–80.

19. Zhang F-J, Chen M-L, Oh W-C. Photoelectrocatalytic properties and bactericidal activities of silver-treated carbon nanotube/titania composites. Compos Sci Technol. 2011;71(5):658–65.

20. Wei LQ, Chen XL, Gao XH, Guo RJ, Xu BS. Preparation of Ag/SiO2 powder with light color and antibacterial performance. Powder Technol. 2014;253:424–8.

21. Baheiraei N, Moztarzadeh F, Hedayati M. Preparation and antibacterial activity of Ag/SiO2 thin film on glazed ceramic tiles by sol–gel method. Ceram Int. 2012;38(4):2921–5.

22. Kim YH, Lee DK, Cha HG, Kim CW, Kang YS. Synthesis and characterization of antibacterial Ag−SiO2 nanocomposite. J Phys Chem C. 2007;111(9):3629–35.

23. Avivi S, Mastai Y, Gedanken A. Sonohydrolysis of In3 + Ions: formation of needlelike particles of indium hydroxide. Chem Mater. 2000;12(5):1229–33.

24. Ishida T, Kuwabara K, Koumoto K. Formation and characterization of indium hydroxide films. J Ceram Soc Jpn. 1998;106 (1232):381–4.

25. Bauer AW, Kirby WM, Sherris JC, Turck M. Antibiotic susceptibility testing by a standardized single disk method. Am J Clin Pathol. 1966;45(4):493–6.

26. Tubtimtae A, Lee M-W. ZnO nanorods on undoped and indium-doped ZnO thin films as a TCO layer on nonconductive glass for dye-sensitized solar cells. Superlattices Microstruct. 2012;52 (5):987–96.

27. Sena C, Costa MS, Muñoz EL, Cabrera-Pasca GA, Pereira LFD, Mestnik-Filho J, et al. Charge distribution and hyperfine interactions in the vicinity of impurity sites in In2O3 doped with Fe Co, and Ni. J Magn Magn Mater. 2015;387:165–78.

28. Anandan S, Vinu A, Mori T, Gokulakrishnan N, Srinivasu P, Murugesan V, et al. Photocatalytic degradation of 2,4,6-trichlorophenol using lanthanum doped ZnO in aqueous suspension. Catal Commun. 2007;8(9):1377–82.

29. Zhu W, Zhai J, Sun Z, Jiang L. Ammonia Responsive Surface Wettability Switched on Indium Hydroxide Films with Micro- and Nanostructures. J Phys Chem C. 2008;112(22):8338–42.

30. Li Y, Lei R, Xu S. Effect of pH on the synthesis of In(OH)3 and In(OH)3:Ce3+/Dy3+ nanocrystals by a fast, mild microwave method. J Solid State Chem. 2018;258:117–23.

31. Mikhlin YL, Pal'yanova GA, Tomashevich YV, Vishnyakova EA, Vorobyev SA, Kokh KA. XPS and Ag L3-edge XANES characterization of silver and silver–gold sulfoselenides. J Phys Chem Solids. 2018;116:292–8.

32. Kőrösi L, Papp S, Dékány I. Preparation of transparent conductive indium tin oxide thin films from nanocrystalline indium tin oxide by dip-coating method. Thin Solid Films. 2011;519 (10):3113–8.

33. Ho WH, Yen SK. Preparation and characterization of indium oxide film by electrochemical deposition. Thin Solid Films. 2006;498(1):80–4.

34. Nakamoto K. *Theory of normal vibrations. Infrared and Raman Spectra of Inorganic and Coordination Compounds*. Hoboken, NJ: John Wiley & Sons; 2008:1–147.

35. Motta FV, Lima RC, Marques APA, Leite ER, Varela JA, Longo E. In2O3 microcrystals obtained from rapid calcination in domestic microwave oven. Mater Res Bull. 2010;45(11):1703–6.

36. Motta FV, Lima RC, Marques APA, Li MS, Leite ER, Varela JA, et al. Indium hydroxide nanocubes and microcubes obtained by microwave-assisted hydrothermal method. J Alloy Compd. 2010;497(1):L25–8.

37. Zhu H, Wang Y, Wang N, Li Y, Yang J. Hydrothermal synthesis of indium hydroxide nanocubes. Mater Lett. 2004;58 (21):2631–4.

38. Lin S-E, Wei W-CJ. Synthesis and growth kinetics of monodispersive indium hydrate particles. J Am Ceram Soc. 2006;89 (2):527–33.

39. Shi Z, Wang W, Zhang Z. Synthesis and characterization of indium hydroxide truncated polyhedral microcrystals. Mater Lett. 2008;62(27):4293–5.

40. Motta FV, Marques APA, Li MS, Abreu MFC, Paskocimas CA, Bomio MRD, et al. Preparation and photoluminescence characteristics of In(OH)3:xTb3 + obtained by Microwave-Assisted Hydrothermal method. J Alloy Compd. 2013;553:338–42.

41. Wood DL, Tauc J. Weak absorption tails in amorphous semiconductors. Phys Rev B. 1972;5(8):3144–51.

42. Li H, Meng F, Gong J, Fan Z, Qin R. Structural, morphological and optical properties of shuttle-like CeO2 synthesized by a facile hydrothermal method. J Alloy Compd. 2017;722:489–98.

43. Zhou Z, Liu G, Wei Q, Yan H, Liu Q. Luminescence properties of Ag nanoclusters doped SiO2–PbF2 oxyfluoride glasses. J Lumin. 2016;169:695–700.

44. Zhang A, Zhang J. Visible-light activities of Gd2O3/BiVO4 composite photocatalysts. J Mater Sci. 2010;45(15):4040–5.